

3D-Printed Phase-Change Artificial Muscles with Autonomous Vibration Control

Moslem Mohammadi, Abbas Z. Kouzani, Mahdi Bodaghi, Yong Xiang, and Ali Zolfagharian*

Currently, additive manufacturing is utilized to fabricate many different actuators suited for soft robots. However, an effective controller paradigm is essential to benefit from the advantages of soft robots in terms of power consumption, production costs, weight, and safety while operating near living systems. In this work, an artificial muscle is additively manufactured with soft silicone elastomer material capable of demonstrating several levels of stiffness. The 3D-printed muscle is equipped with carbon fibers to receive a stimulus signal and develop a programmable joint that can present different stiffnesses. A nonlinear controller is developed to autonomously control the variable stiffness joint based on a reinforcement learning algorithm. The controller exhibits a slight increase in settling time; however, it demonstrates a decrease in fluctuation amplitude by 33% and a substantial reduction in power consumption by 41% in comparison to the optimized proportional integral derivative controller. At the same time, it is adaptable to and reliable in new conditions. The variable stiffness muscle is also used as a controllable mechanism to suppress the low frequency vibration. The study shows that the muscle can successfully attenuate the vibration autonomously when it is increased.

1. Introduction

Additive manufacturing (AM) has sparked the attention of engineers and scientists due to its exceptional flexibility and ability to print complicated structures.^[1] The 4D printing fabrications are capable of altering their structure in response to specific environmental signals like electric fields, temperature, magnetic fields, and light.^[2] This feature of 4D printing makes it increasingly popular to fabricate soft actuators and robots.^[3] Additionally, the use of 4D printing technology offers advantages for addressing a number of factors, including decreasing overall fabrication costs and assembly time.^[4,5] In the developing 4D printing technology, researchers employ a variety of materials, including magnetic material, hydrogels, and shape memory polymers (SMP).^[6,7]

Traditional manufacturing techniques have so far been used to create a significant number of robots for a range of industrial applications while high energy consumption and material waste rates are two of these technologies' most noteworthy flaws.^[8] Researchers, however, are investigating new techniques and processes to manufacture soft robots and actuators to address the drawbacks of existing rigid robots.^[9,10] In comparison to other manufacturing processes, 4D printing could be seen as being noticeably advantageous in producing soft robots. One of the many routine jobs performed by robots is frequently manipulating objects in different shapes around them.^[11] The 3D-printed soft actuators frequently resemble human limbs with several degrees of freedom (DoF).^[12] These robots can be labeled as rigid or flexible limbs. Robotic manipulators with frames composed of steel or aluminum are common because of their high tensile strength. On the contrary, these robots will be inflexible and hefty.

Growing demand for portable, lightweight robotic arms as well as developments in material science and robotics, have inspired research on the design, fabrication, and manipulation of flexible robotic arms. Flexibility is provided by utilizing plastic, compliant mechanisms, or carbon-fiber frames, which significantly reduce the cost of production and the robot's energy consumption. Additionally, soft robotic grippers are significantly more efficient at handling fragile or irregularly shaped objects than traditional rigid grippers. The main limitations of such systems are their

M. Mohammadi, A. Z. Kouzani, A. Zolfagharian
School of Engineering
Deakin University
Geelong, Victoria 3216, Australia
E-mail: a.zolfagharian@deakin.edu.au

M. Bodaghi
Department of Engineering
School of Science and Technology
Nottingham Trent University
Nottingham NG11 8NS, UK

Y. Xiang
School of Information Technology
Deakin University
Geelong, Victoria 3216, Australia

 The ORCID identification number(s) for the author(s) of this article can be found under <https://doi.org/10.1002/admt.202300199>

© 2023 The Authors. Advanced Materials Technologies published by Wiley-VCH GmbH. This is an open access article under the terms of the Creative Commons Attribution-NonCommercial License, which permits use, distribution and reproduction in any medium, provided the original work is properly cited and is not used for commercial purposes.

DOI: 10.1002/admt.202300199

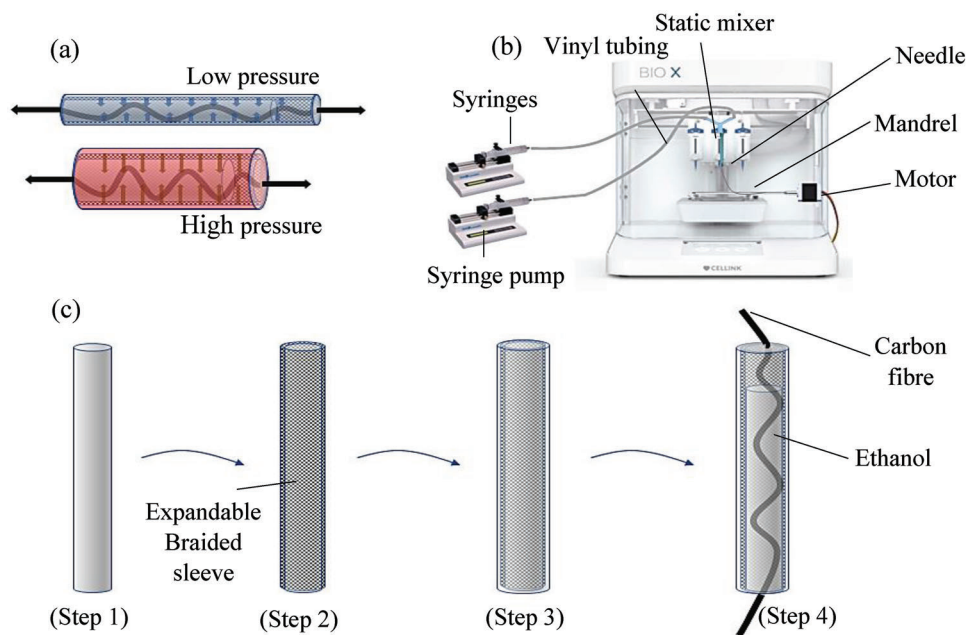


Figure 1. a) The phase transitioning muscle in low/high-pressure conditions. b) Modified printer for silicone mandrel printing c) Silicone cylinder printed on the mandrel (Step 1). Covering the silicone cylinder with extendable braided sleeve (Step 2). Printing silicone layers to cover the sleeve (Step 3). Removing the mandrel, inserting the carbon fiber, and filling the chamber with ethanol (Step 4).

limited range of gripping power and inability to execute diverse tasks in diverse surroundings. Researchers have proposed variable stiffness structures and specific designs to overcome these limitations.^[13–15] One of the most popular soft actuators is pneumatic actuator, which can provide a high force-to-weight ratio by adjusting the pressure inside the actuator chamber.^[16] In addition, this actuator can provide variable stiffness when the chamber pressure is changed. **Figure 1a** shows a pneumatic chamber in a low and high-pressure situation, respectively. When the stretching force is applied to the muscle, it converts to the compressing force on the fluid inside the chamber. Therefore, the required force to stretch the muscle to a specific amount varies in different conditions.

The additive-manufactured soft pneumatic actuators (SPAs) can produce complex movements, including jumping, bending, and twisting, in response to the changing pressure in their chamber.^[17] In refs. [18–21], the authors develop a pneumatic actuator that activates through high-pressure fluid provided via pumping through AM to reduce manufacturing time and cost while providing various features, such as self-healing, precise actuation, and size customization. The flexible joints can be equipped with SPAs to provide multi-level variable stiffness joint autonomously. However, the integration of pump and pipes into the SPAs systems often results in increased weight and bulk. Researchers have proposed the implementation of phase transition muscles (PTM) as a mean to eliminate the pump and produce the required pressure through phase transitions. Sangjan et al. proposed an innovative phase change muscle filled with paraffin that could be activated thermally and can achieve 9% contraction.^[22] Another thermally activated muscle was proposed that is filled with ammonia liquid with an embedded heating element to stimulate 17% contraction.^[23] Mirvakili et al. introduced magnetically

activated muscle by filling the muscle's bladder with a liquid-to-gas phase transition liquid and reached 20% contraction.^[24] A flexible phase transition muscle is 3D-printed and evaluated in this paper.

As a result of the robotic arm's flexibility, there can be various levels of inaccuracy, such as more vibration before settling, especially close to the robotic arm's end. Rigid manipulator control methods do not perform well with flexible manipulators. In order to handle the time variant flexible robotic arms, unique algorithms that are exact and efficient must be developed. The two most widely utilized linear control approaches are proportional integral derivative (PID) and linear quadratic regulator (LQR), yet they are not preferred due to the nonlinearity and time variance of the soft variable stiffness actuator.^[25] Using full-state feedback, Akyuz et al. proposed a PID control law to manage a robot arm with a flexible joint.^[26] The PID control methodology can also be combined with various control techniques to develop a more reliable controller and boost system efficiency.^[27] The LQR is another significant and popular technique for controlling robotic arm systems. Since LQR seeks to optimize the quadratic cost, it has gained much popularity due to its simplicity, optimum performance, versatility, and analytical solution. However, in terms of trajectory tracking, LQR and PID replies are equivalent.^[28] Nevertheless, the core controller for the industry still uses linear approaches because of their simplicity.^[29]

Other than PID and LQR, researchers investigated a variety of nonlinear techniques to develop a controller for flexible joint robots, including fuzzy logic,^[30–33] neural networks (NN),^[34] and neuro-fuzzy logic.^[35] Additionally, flexible connections and joint link mechanisms are controlled by the RL approaches.^[36–39] RL is a technique used in the control area to create adaptive controllers that could learn in real-time and become close to the desired

controller. A reward-penalty strategy is used by RL to respond to the input and feedback signal to control the system. The controller modifies its behavior to maximize rewards. This approach makes it possible to design a type of adaptive controller without having complete system dynamics information where the optimized controller can be developed by solving the Hamilton–Jacobi–Bellman equations online.^[38]

Despite the extensive research on 3D printing of various materials, including silicone, the 3D printing of silicone on a mandrel is a novel area of research with its own unique set of challenges. One major challenge is the viscosity of the silicone; if it is too low, the silicone may become runny, while if it is too high, it requires excessive pressure to be extruded. Additionally, controlling the movement of the mandrel and tailoring the G-code to the mandrel system is also a challenge. Another gap in this field is the development of a proper controller for non-linear systems, such as soft joint robots. Deep reinforcement controllers (DRL) have been identified as a significant solution, however, they also come with their own challenges, including the appropriate sizing of the deep neural network (DNN), which must balance between satisfying the complexity of the system and having the desired level of flexibility at the output. Furthermore, designing an effective reward function is critical for a successful reinforcement controller.

This research aims to develop innovative mechanisms with variable stiffness characteristics through additive manufacturing (AM) and address the control challenges associated with soft and flexible structures. The unique aspect of this work lies in the combination of three key elements: 3D printing the silicone chamber on a mandrel, developing a reinforcement learning (RL) controller for variable stiffness structures, and utilizing the structure in attenuating vibration. By utilizing 3D printing, the design of the PTM is customizable, the cost of manufacturing is significantly reduced, and achieving different stiffness levels is easily attainable by changing the pressure inside the printed actuator chamber. The development of an RL controller is an innovative approach to controlling compliant systems, which allows for improved adaptability and reliability. Additionally, this work aims to evaluate the PTM's capability to suppress low-frequency vibrations similar to human limb tremors, which is a novel application for this type of technology. Overall, this research presents a novel approach to designing and controlling flexible manipulators and compliant systems, utilizing 3D printing and RL controllers to achieve variable stiffness characteristics and suppress vibrations.

2. Results and Discussion

This paper offers a technique for utilizing the DRL method to design a controller to improve the precision of trajectory tracking in a robotic arm with a 3D-printed variable stiffness joint. Additionally, the intention is to reduce power consumption, arm vibration, and track errors. Furthermore, the variable stiffness structure is exploited to attenuate the limb's tremor upon demand. The experimental setup is assembled by a motor-driven rigid beam that is equipped with two 3D-printed PTMs to provide flexibility to the joint. The PTMs can express variable stiffness to increase the range of flexibility of the joint. The PTMs chamber is filled with ethanol and applying a low voltage to the integrated carbon fiber string can change the chamber's stiffness. BIO X—3D

bioprinter—CELLINK is modified to print the silicone chambers of the PTM (Figure 1b and Movie S1, Supporting Information).

First, two 16-gauge syringes are filled with Ecoflex 00–50 parts A and B separately with thivex additive and loaded into the syringe pumps. The pump pushes the material through the vinyl tubes to the static mixer, which is fixed on the printer instead of the main nozzle. The static mixer allows input flows to be properly mixed and releases the Ecoflex mixture at the output through the dispensing needle with a 1.27 mm inner diameter. Thin layers of silicone are printed on the mandrel, while a stepper motor controls the mandrel. The needle was moved parallel to the mandrel axis at a fixed distance from the surface, while the mandrel is rotated at a constant speed to deposit multiple silicone layers (Figure 1c-Step 1). Then an expandable braided sleeve is manually worn on top of the layers (Figure 1c-Step 2), and the printing of the silicone is continued to cover the sleeve (Figure 1c-Step 3). The braided sleeve is able to convert the expansion force in the chamber to the contraction force.

3D printing of the chamber offers several advantages over traditional manufacturing methods when creating a flexible phase transitioning muscle. First, it decreases the cost of manufacturing by eliminating the need for casting molds and using less material. Second, the structure of the muscle is customized using 3D printing. For example, instead of uniform wall thickness, the thickness of the wall is changed in specific parts to provide more complex movement instead of just linear contraction. This would typically require the use of various cast shapes for different movements, which is both time-consuming and expensive to manufacture. Last, the expandable braided sleeve can be printed simultaneously with the silicone printing with a different pattern. This allows for the creation of intricate designs that would be difficult to achieve with traditional methods.

After printing, the 3D-printed silicone chamber is filled with ethanol, and the carbon fiber is inserted into the chamber (Figure 1c-Step 4). The carbon fiber heating wire with 33 ohm m⁻¹ resistance that can endure up to 200 °C. By integrating the carbon fiber, the muscle is capable of being stimulated with low voltage to evaporate ethanol and increase the chamber's pressure. In the last step, both sides of the chamber are sealed with a thicker layer of silicone, 90% of the chamber is filled with ethanol, and 10 cm of the carbon fiber is inserted into a 7 cm length chamber. The internal diameter of the muscle is 7 mm, the outer diameter is 10 mm, the length is 70 mm, and ≈2.5 mL of ethanol is poured into the muscle.

Various experimental processes are conducted to assess the performance of the additively manufactured artificial muscle. In the first experiment, one end of the muscle is fixed, and the other end is relaxed (Figure 2a). Then a constant voltage is applied to examine the maximum contraction of the muscle. In another experiment, a weight equal to 130 g is attached to the relaxed end to evaluate the contraction of the muscle under an external force equal to 1.3 N (Figure 2b).

In the first experiment, the relaxed muscle is to reach a 28.6% contraction. This contraction is obtained in 56 s when the muscle is activated by 5 V. In addition, the same contraction occurs in 39 s while 8 V is applied to the muscle. The extension and contraction of the muscle are repeatable without labor intervention. The experiment is repeated ten times, and the muscle contraction is recorded. Figure 2a shows the boundaries and the average value

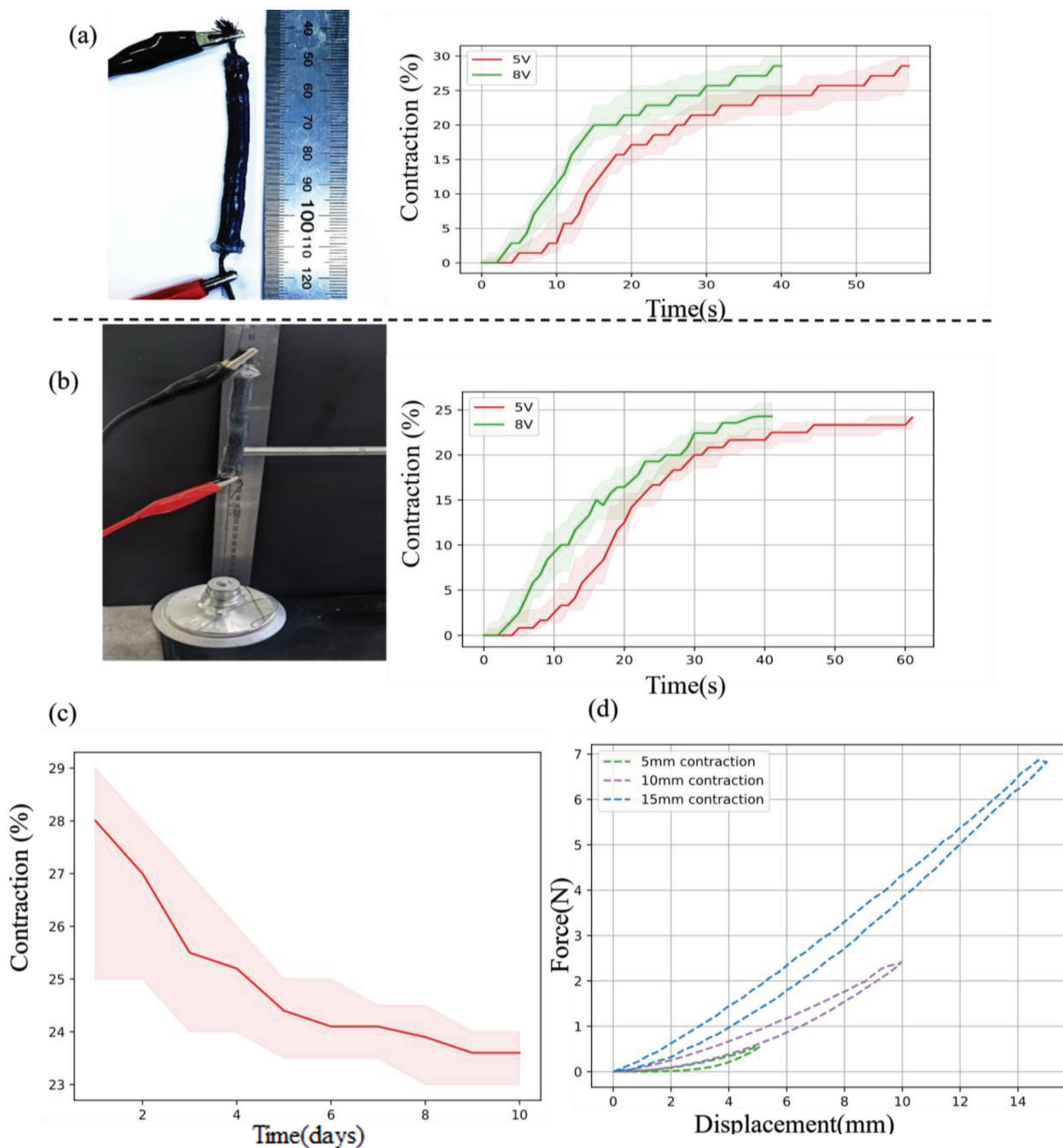


Figure 2. a) Contraction experiment in relaxed condition. b) Loaded contraction. The experiment for both conditions is performed under 5 and 8 V. c) Durability of five muscles in 10 days d) stiffness of the muscle.

of the contraction for this experiment. In the experiment with the 130 g weight, because of the 1.3 N external force (Figure 2b), the contraction of the muscle decreases to 24%. The muscle reaches this contraction in 61 and 41 s for 5 and 8 V, respectively.

The muscle is not equipped with an active cooling system. Therefore, the recovery of the muscle to its initial length is slower compared to its contraction. 33% of the recovery is achieved in 18 s, meaning the muscle length reaches 58 from 53 mm. Sub-

sequently, 32 s is needed to reach 64 from 58 mm. For the full recovery of the muscle from 53 to 70 mm, 110 s is required on average. This time depends on the environment's temperature and could be varied by changing the surrounding temperature, and this experiment is conducted at room temperature (21 °C). Additionally, the contraction time is also dependent on environment temperature, and increasing environment temperature can decrease contraction time. Based on the carbon fiber

characteristics and the experiment's time, the muscle's power consumption can be analyzed.

The consumed energy of the muscle can be calculated based on $W = \frac{V^2}{R}t$, while V is the applied voltage, R is the resistance of the wire, and t is the time for contraction. The resistance of 10 cm wire is 3.3 ohm; therefore, the required energy in the first experiment is 424 and 756 J for 5 and 8 V, respectively. Also, 462 and 795 J are needed in the second experiment to reach 24% of contraction while the 5 and 8 V are applied, respectively. The results show that even though the contraction is obtained faster by applying higher voltages, the amount of consumed energy is higher. Therefore, the applied voltage can be chosen based on the application of the muscle. If a higher speed of contraction is needed, higher voltages must be applied. Nonetheless, if the muscle must be run on low-capacity batteries, the voltage can be decreased to reduce power consumption. However, the limitations of carbon fiber in handling high voltages and currents must be considered.

A power regulator was utilized to power the controller (Arduino) and the PTM from a portable power source. This enables the precise control of the voltage applied to the muscle by controlling the power switch (TIP120 transistor), allowing for a more accurate and consistent performance. The power consumption of the muscle is 500 J per cycle on average, and a 9 V alkaline battery stores around 20 000 J. This amount of energy is sufficient to power the muscle for 40 cycles. In practice, the battery provides 30 cycles on average (Figure S1, Supporting Information). Lithium-ion (Li-ion) batteries are better options because they are rechargeable and store a higher amount of energy with a similar weight. Another muscle parameter is the outer temperature of the muscle, which is important in wearable applications. During the experiment with the weight, the external side temperature of the muscles is recorded. The surface's temperature increases gradually, reaching 40 °C when the muscle has a 12 mm contraction equal to 17% contraction. When the heating continues to get a higher contraction, the soft muscle finally obtains a 24% contraction while the surface temperature reaches 50 °C. Even though this temperature is uncomfortable if it touches bare skin, it could be utilized with a lower contraction rate or worn into fabrics to avoid direct touch.

In order to assess the stiffness of the muscle, tensile tests were performed on the PTM under varying states of contraction. The results of these tests, depicted in Figure 2d, demonstrate the muscle's response in 5, 10, and 15 mm contractions. Higher levels of contraction could be achieved by increasing the pressure within the chamber, resulting in greater levels of stiffness. Notably, the stiffness of the muscle at low levels of contraction (5 mm) is 110 N m⁻¹, while a stiffness of 700 N m⁻¹ was measured in average for the muscle exhibiting 20 mm contraction which means its stiffness increases 6.36 times. Table S1, Supporting Information shows various variable stiffness materials compared to the PTM. The durability of the PTM is a crucial factor that demands evaluation owing to the silicone's permeability. To this end, five muscles were produced, and the contraction experiment (unloaded) was conducted for 10 days. The contraction percentage was recorded during this period, as depicted in Figure 2c, which revealed a decreasing trend from 28% to 24%. Although the PTM demonstrated substantial contraction, its permeability must be reconsidered in future research.

In the simulation environment (Supporting Information, Appendix 4), the DDPG and TD3 are set to be trained. The reward function is calculated at every step, and the accumulated reward of these steps is calculated in every episode. The accumulated reward is displayed in Figure 3 for both agents. The blue line shows every episode's reward, and to see the training trend in the training phase (Figure 3a,c), a moving average filter with a length of 50 is applied to the data shown in orange color. The trends in Figure 3a,c are both upward trends that indicate the controllers are improving their ability to control the system and acquire more rewards. In other words, the controllers follow the desired track better and decrease the vibration of the beam at the same time. The reward function is used on the PID controller to calculate the accumulated reward for this controller to make a stop criterion. Therefore, the calculated amount is used to stop training when the RL controllers can collect more rewards in one episode than the PID controller. As shown in Figure 3, the accumulated reward sometimes drops because the agent is exploring various options to find the best way to control the system.

After training the RL agents (DDPG and TD3), the controllers apply to control the Quanser system to follow the step function, and the motor angle is shown in Figure S3a, Supporting Information (Appendix 1) compared to the response of the PID controller. DDPG and PID controllers are outperformed by the TD3 controller in terms of the rise time (1.27, 1.24, and 1.21 s, respectively). However, the PID settles more quickly (1.38 s) than alternative controllers (DDPG: 1.44 s, TD3: 1.62 s).

The manipulator fluctuation angle is shown in Figure S3b, Supporting Information (Appendix 1) for all the controllers. Although the RL controllers' fluctuation persists longer, the PID-controlled manipulator's vibration has a higher peak (PID: 0.18 rad, DDPG: 0.10 rad, TD3: 0.08 rad). Additionally, RL algorithms require less action (applied voltage on the motor) than the PID controller. The total of the squared voltage values (that is directly proportional to the power consumption) for TD3 and DDPG is equal to 1 and 1.25, respectively, in terms of power consumption. The PID controller's consumption is proportional to 1.97, which is nearly twice as much as the required power for the TD3 controller.

The joint stiffness is reduced to evaluate the controllers' behavior under the new circumstances after investigating the effectiveness of various controllers on the system. The PID and TD3 controllers' responses are displayed in Figure S4, Supporting Information (Appendix 1). The controllers produce an acceptable outcome despite being adjusted to various conditions. In contrast to the PID controller, the TD3 has a better response time. The RL agent overshoots by 8.2%, whereas the linear controller overshoots by 11.8%. Additionally, TD3 has a rise time of 1.01 s, which is faster than the PID controller's 1.20 s. Additionally, the manipulator's oscillation boundary for both controllers is raised.

The RL agent can learn and adjust to new circumstances regardless of the outcome depicted in Figure S4, Supporting Information (Appendix 1). As a result, the agents were retrained, and Figure 3b,d depict the episode reward from the retraining phase. In a few episodes, RL agents can adjust to the new system. The TD3 is evaluated after retraining in order to contrast with the PID controller. The system's reaction after using the step function is seen in Figure 4a shows that the DRL controller performs better than the result in Figure S4, Supporting Information (Appendix

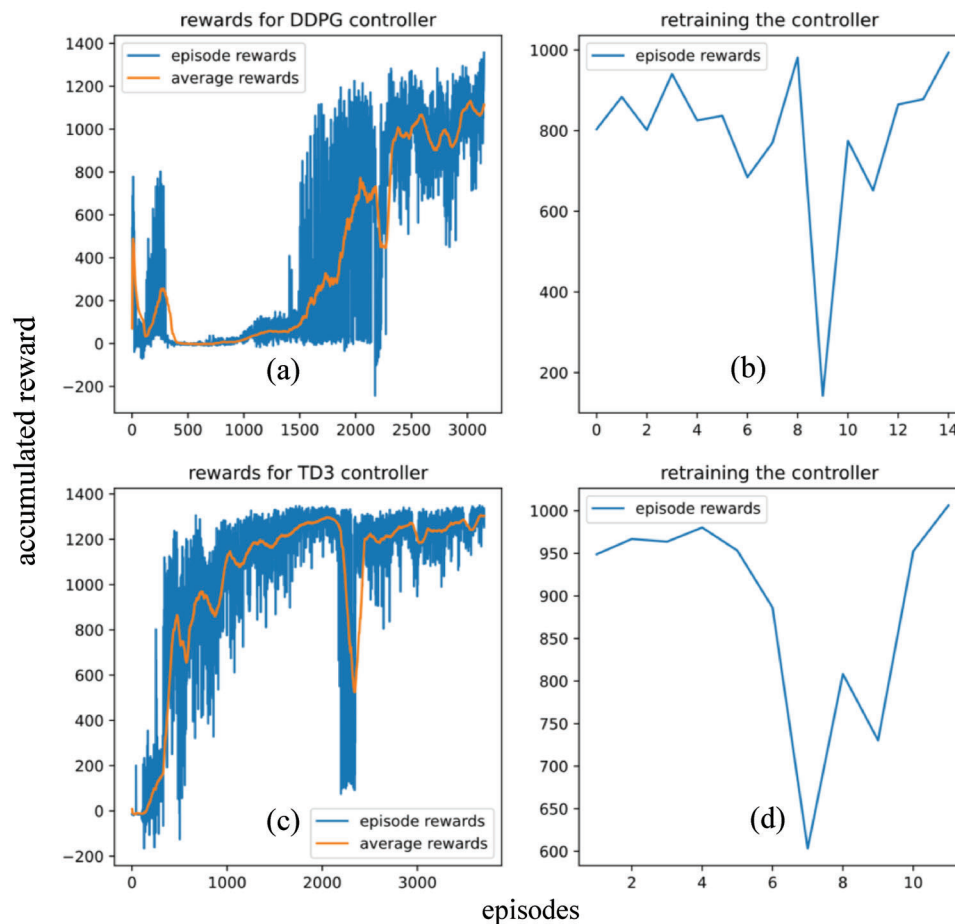


Figure 3. The accumulated reward of the agent during the training and retraining phase. a) Episode accumulated reward during training for the DDPG agent. b) Retraining episode reward for the DDPG. c) Episode accumulated reward during training for the TD3. d) Retraining episode reward for the TD3.

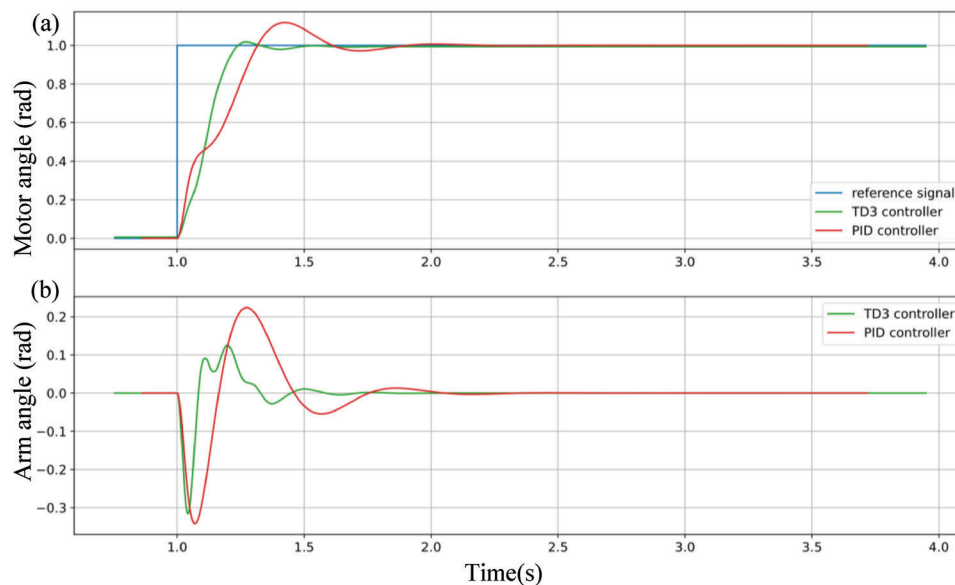


Figure 4. PID and TD3 controllers' performance after decreasing the stiffness of the joint and retraining the RL agent. a) Motor angle under TD3 and PID controller to track the reference signal. b) Robot's arm oscillation.

1), while the PID controller remains unchanged. As a result, the outcome is consistent with the previous experiment, but the RL controller's rising time is improved. The link settles more quickly than in the previous edition, which means that the retraining improved the link's oscillation.

To assess the muscle as a variable stiffness mechanism and the developed RL controller in an experiment, a setup, including five main parts is exploited. The setup includes 1) Rotary Servo Plant: Quanser SRV02 and Rotary Flexible Joint: Quanser ROT-FLEX Module. 2) Power Amplifier: Quanser VoltPaq-X1. 3) Matlab/Simulink software. 4) Data Acquisition Board: Quanser Q2-USB and 5-power supply (Figure 5a). The spring is switched out for the 3D-printed silicone muscle with a variable stiffness mechanism that is capable of changing the stiffness directly by applying voltage to the integrated carbon fiber. The experiment uses a sampling rate of 40 samples per second (0.025 s). The incremental encoder sensor, which is a part of the Quanser unit, may generate up to 4096 pulses each cycle and is used to calculate the position of the rigid arm. The rotator and the rigid arm displacement and angular velocity are provided to the RL algorithm as the feedback signal. Critic and actor DNN have a similar architecture, including two hidden layers with 20 and 10 nodes each that can provide a suitable controlling signal for the system.

Figure 6a shows the motor angle as the controller tries to track the step function (see Movie S2, Supporting Information), in this case rotating the arm by 45° (or $\pi/4$ rad) as part of the experiment. According to the graph, the rise time for the PID controller is 0.22 s, which is almost equal to the rise time for the TD3. The rise time for the DDPG controller is 0.27 s, making it slower than the other controllers. The overshoot for DDPG controllers is negligible, but the TD3 and PID controllers show an overshoot of 7% and 2%, respectively.

Figure 6b depicts the rigid arm's oscillation. It shows that PID controller vibration in the joint will be dampened sooner than the other approaches, comparable to the simulation. However, the RL controllers' oscillation magnitude, particularly that generated by the DDPG agent, is less than the PID's response. Then, the experiment is repeated with a different spring stiffness by applying the stimulus signal through the carbon fiber to assess the effectiveness of the controller under various conditions. The soft muscle's temperature is changed, and then the pressure inside the silicone's chamber is altered. The stiffness of the muscle

is adjusted following the pressure change. In order to effectively control the system during this experiment, the TD3 algorithm's settings are set to learn the new condition online.

Figure S5, Supporting Information (Appendix 1) demonstrates that the retrained TD3 can control the system more accurately than the PID controller because its parameters suit the new condition. Compared to the PID controller, the TD3 controller is quicker and has a shorter rise time (0.21 and 0.26 s, respectively). Additionally, the PID controller's overshoot is around 5%, and the RL agent has a 6.4% overshoot. In the new experiment, the muscle's temperature is reduced, therefore, the joint's stiffness is reduced compared to its original state, and it causes a more significant fluctuation of the joint under the supervision of the unchanged PID controller (see Movie S3, Supporting Information). However, it still dissipates more quickly than the oscillation connected to the RL controller. Once more, when the RL controller is in control of the system, the link's fluctuation magnitude is less severe. The voltage signal provided to the amplifier in the experiment served as the basis for calculating power usage. Based on the signal, the PID controller's power consumption is 1.69 times more than the TD3 controllers.

This study shows that the variable stiffness PTM gives our system several levels of stiffness without requiring human labor to take the structure apart and add new components. Despite its benefits, there are still a few issues that could be covered in the following works. The next phase in the 4D printing process involves co-printing the carbon fiber to decrease human intervention in the fabrication process of the muscle. Another obstacle that might need to be addressed in order to incorporate the variable stiffness structure into wearable technology is replacing the ethanol with materials with a lower boiling point temperature; therefore, the muscle could be activated at lower temperatures, which leads to lower energy consumption as well. The improved performance was attained by creating the DRL agent to control the variable stiffness joint. Without human involvement, the system was able to adjust to new settings. The controller also considerably reduces power usage, which is a huge benefit for using it in portable devices.

By combining the adaptive controller with the time variable system, the output may be used in a broad range of applications. In order to gain higher efficiency, most wearable devices, including prosthetics, rehabilitation equipment, and assistant systems,



Figure 5. The experimental setup 1) Laptop/Matlab software. 2) Data Acquisition Board. 3) Power Amplifier. 4) Flexible joint Quanser unit equipped with the PTM. 5) Power supply.

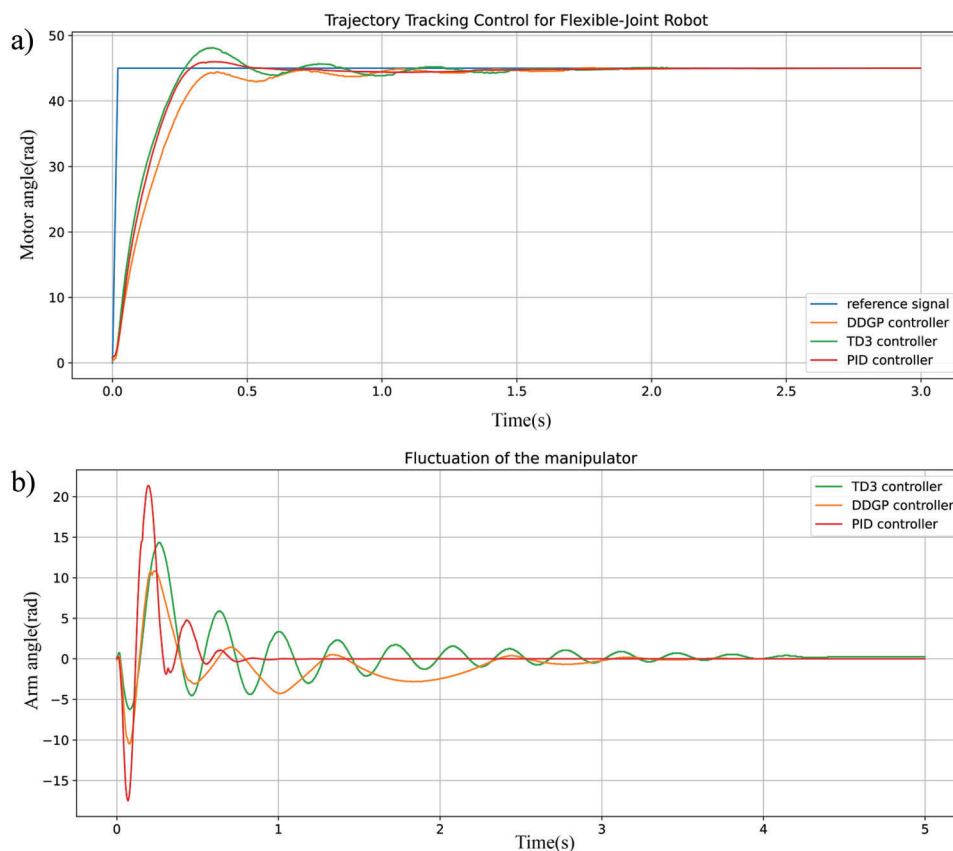


Figure 6. a) Motor's angle response to step function controlled under linear and nonlinear controllers in the experiment. b) Manipulator's endpoint fluctuation angle in the step response under linear and nonlinear controllers in the experiment.

must include a variable stiffness mechanism. The individuals who are wearing the gadget want their organs to show different features in various situations; therefore, the gadget must be a time-variant structure. Another issue is the amount of power that wearable technology consumes.^[40] In comparison to a conventional controller, the device might run longer with the designed nonlinear controller suggested in this research while using the same quantity of attached battery.

An application of the PTM component with variable stiffness in human limb orthosis is shown in **Figure 7** to suppress upper limb tremors. The variable stiffness glove can be actuated by applying electric power to the silicone muscles, and RL agents control their temperature while the artificial soft muscles are placed alongside the limb muscle. The gadget is more user-friendly because of its lightweight and softness. While the upper limb starts vibrating, the temperature is raised to increase stiffness in the structure. But increasing the stiffness, the passive force of the artificial muscle will decrease the tremor of the arm. A significant problem with wearable technologies is their weight.^[40] A lightweight wearable gadget can be achieved by reducing the device's power consumption, which also reduces the bulk of the battery. Additionally, the design of the PTM offers a distinct advantage over pneumatic muscles in terms of weight and volume reduction. This is due to the absence of the need for fluid pump connections.

Compared to traditional tremor suppression gloves, this glove has several advantages. First, it weighs less and is more flexible,

making it more comfortable and user-friendly. Second, the design is more general and can be customized for specific tremors in different parts of the upper limb, including flexion–extension, radial–ulnar, or pronation–supination motion.^[40] In individuals with flexion–extension tremor, for instance, the muscles associated with the tremor are located between the forearm and hand on the dorsal and palm sides, and the artificial muscle is placed parallel to that. When the tremor is detected, the controller stimulates the artificial muscle to achieve higher stiffness, which dissipates the oscillating movement of the muscle similar to ref. [41]. Although the mechanism may affect voluntary motion, the voluntary force is typically higher than the tremor forces. Therefore, the individual can still perform their task while the tremor force is dissipating. Regarding the voltage control of the PTM, the controller obtains feedback from the tremors and the PTM temperature utilizing sensors. When a tremor occurs, the controller adjusts the voltage on the muscle via an adjustable voltage booster to increase its stiffness. When the tremor subsides to a reasonable level, the controller maintains the pressure by controlling the temperature.

On the same setup, a different experiment is done to test how well the muscle stops the low frequency vibration similar to human arm tremor. In this experiment, the silicone muscle is added to the springs in the parallel position instead of replacing them on the Quanser flexible joint unit. Upper limb tremors can occur at various frequencies and amplitudes. However, the most common frequency is 4 Hz. Therefore, in the experiments,

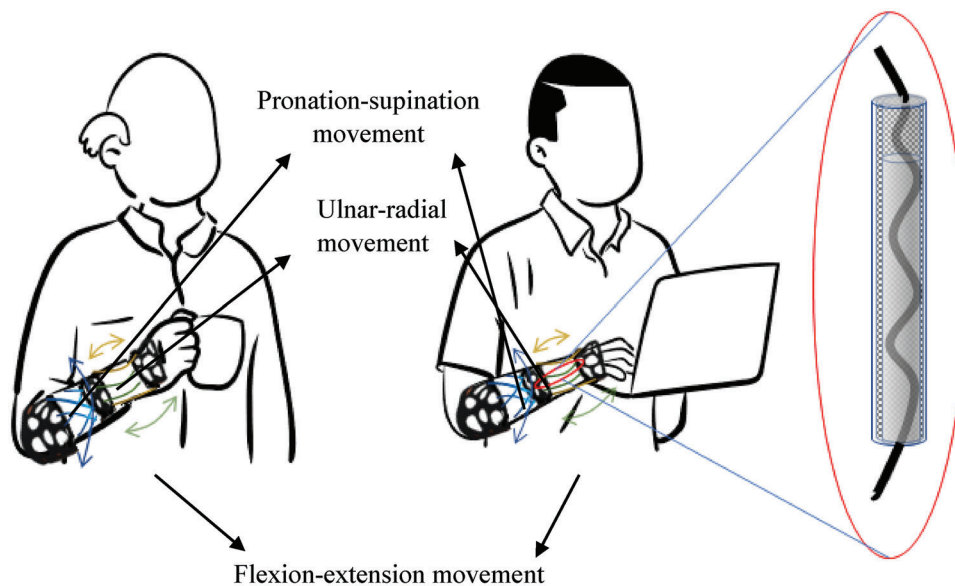


Figure 7. Variable stiffness PTM glove to suppress tremors in forearm and hand.

various sinusoidal signals with 4 Hz frequency and two different amplitudes are applied to the motor to generate low frequency vibration to mimic human arm tremor. When the motor's gear starts to move, the muscles are in an idle state. As a result, the rigid arm can move in a semi-sinusoidal motion with the primary frequency equal to the motor (4 Hz). The artificial muscles are activated to suppress the vibration in the rigid arm. The activated muscle makes the joint stiffer, which causes a decrease in the vibration of the Quanser unit arm, as shown in **Figure 8** and **Figures S6** and **S7**, Supporting Information (Appendix 1).

Figure 8a,b show that when the muscle is added to the flexible joint with 15° vibration amplitude, even in idle mode, it affects the vibration amplitude. Nevertheless, compared to the suppression in the active mode is less than half. The result shows 21.75% and 47.32% suppression for idle and active mode, respectively. **Figure S6a,b**, Supporting Information (Appendix 1) depict the repeatability of the muscle. The difference between various trials is negligible, with an equal amount of vibration attenuating. **Figure S6c,d**, Supporting Information (Appendix 1) illustrate the idle mode of the muscle before activating and after cooling down in the 120 s. The lack of an active cooling system delays the cooling phase and takes longer compared to its activating phase. Despite that, the pictures represent the same suppression percentage in both trials.

The experiments are repeated for a vibration with a higher amplitude equal to 60°, shown in **Figure 8c,d** illustrate the comparison of the effect of the muscle in active and inactive mode. Compared to the vibration with lower amplitude, the muscle performs better with more severe vibration, and the suppression in the idle mode is much smaller than in the active mode. It can reduce the vibration by 14.75% in idle mode, while 81.88% of the vibration is suppressed in activated mode. **Figure S7a,b**, Supporting Information (Appendix 1) represent the performance of the muscle in inactive mode before activating and after cooling down in 120 s with a minor difference.

Based on the result of suppression vibration, the muscle can be a great candidate for wearable devices to suppress tremor be-

cause of its flexible and friendly structure while it has a small volume and being lightweight. Nevertheless, 3D-printed soft robots require further development before they can be used as ubiquitous technology. Exploration of the field of AM and soft robotics, which is viewed as a breakthrough technique, will help disclose new possibilities in various industries in the coming years. Compared to rigid actuators, soft actuators are more sophisticated due to their high degrees of freedom. In order to use soft robotics in a wide range of applications, new controlling paradigms need to be investigated together with the soft robot's development.

3. Conclusion

This article discussed the manufacturing of flexible silicone muscle through additive manufacturing and evaluated its features, including contraction, repeatability, recovery time, and power consumption. The 3D-printed silicone muscle was integrated with carbon fiber string; therefore, it can be activated with a low-voltage signal as the stimulus signal. The variable stiffness characteristic of the muscle was introduced and utilized to develop a variable stiffness joint robot. The variable stiffness joint robot was controlled using the developed RL method using the reward function optimization concept. The experimental apparatus for assessing the controller was a rigid arm with a flexible joint based on the 3D-printed variable stiffness muscle.

When the system's features varied, the controller learnt to adapt to new conditions online. The RL controller's rise time changes from 0.26 to 0.27 s (after retraining), but the identical parameter for RL raises from 0.26 to 0.33 s when the stiffness of the joint changes. Additionally, compared to its linear version, the RL's oscillation and power consumption are reduced by 56% and 58%, respectively. Also, the developed muscle was used in an experiment to suppress vibrations similar to tremors in the human upper limb. By increasing the stiffness of the muscle when the vibration occurs, the vibration's amplitude is decreased up to 81.88%. Also, its repeatability and recovery in suppressing vibration were assessed.

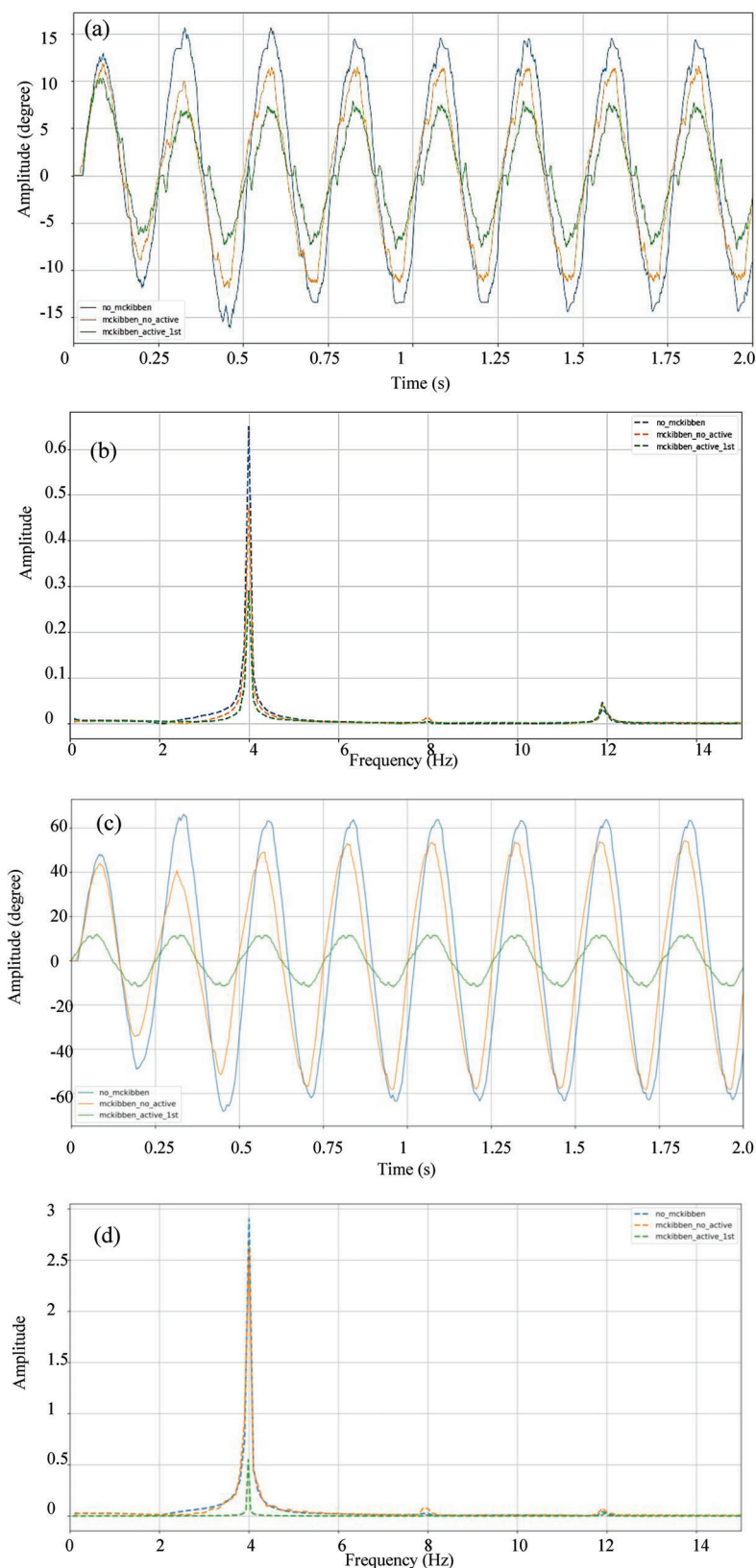


Figure 8. Suppressing tremor with 15° and 60° amplitude by silicone muscle. a) Comparison of the 15° vibration in various situations in the time domain: 1) Without the muscle. 2) Muscle is added in the idle mode. 3) Muscle is activated. b) The same comparison of the vibration suppression in the frequency domain. c) Comparison of the 60° vibration in various situations in the time domain: 1) Without the muscle. 2) Muscle is added in the idle mode. 3) Muscle is activated. d) The same comparison of the vibration suppression in the frequency domain.

The combination of 4D printing of soft actuators with reliable and adaptable controllers empowered by RL algorithms offers a promising outcome with a low energy consumption rate for future cutting-edge and creative applications.

4. Experimental Section

Materials: 1) Ecoflex 00–30: Platinum-catalyzed silicone material with part A and part B. Platinum catalyst and silicones were included in component A, whereas component B held the cure inhibitor, cross-linker, and polymer. 2) THI-VEX: a silicone thickener that is added to Ecoflex silicones in a weight-based manner. 3) Carbon fiber: the Hefei Minco Heating Cable Co carbon fiber heating wire with 33 ohm m⁻¹ resistance and 3 mm thickness contains 12 000 threads that can endure up to 200 °C. 4) Expandable sleeve: expandable sleeving made from PET (polyester) monofilament yarns. 5) Ethanol: volatile and colorless liquid (CH₃–CH₂–OH).

Fabrication of Soft Actuator: The silicone was prepared by mixing 1A:1B by volume. It had a low viscosity to ensure easy mixing and degassing. In the printing processes, higher viscosity was required that was achieved by adding 2% thivex by volume. Therefore, 10 mL of part A and part B were added to two syringes separately. 0.2 mL of thivex was added to each syringe to increase the viscosity. The syringes were loaded into the syringe pumps to push through the static mixer. The dispensing speed of the silicone was set to 10 mL s⁻¹. The needle inner diameter was 1.27 mm, and the nozzle speed is 13 mm s⁻¹. Further aid in curing was provided by a 24 W ceramic heater after printing the silicone. The cured printed silicone was covered with expandable sleeve and the same procedure was continued until the sleeve was covered with a thin layer of the silicone. The curing of the silicone was assisted by using the heater again. The printed silicone was unloaded from the mandrel and the carbon fiber with the length of 10 mm was inserted into the printed structure. Both sides of the structure were covered with silicone to enclose the chamber, then 2.5 mm ethanol was injected into the inner chamber.

Contraction Characterization: The contraction of the artificial muscle was evaluated through two experiments. In the first experiment, one end of the muscle was fixed while the other end was relaxed, and a constant voltage was applied to measure the maximum contraction. POWERTECH 0–30Vdc 5A regulated power supply was used to apply voltage on the muscle and a Keji Stainless Steel Ruler 30 cm was used to measure the size of the muscle. Another experiment measured the muscle's ability to contract in response to an external force by attaching a 130 g weight to the relaxed end. In both experiments, 5 and 8 V were applied to the muscle and these experiments were repeated to check the muscles performances.

Muscle Recovery: The muscle recovery was performed in the room temperature 21 °C. To conduct the experiment the PTM was activated, then the power supply (POWERTECH 0–30Vdc 5A) was turned off. The length of the PTM was measured by utilizing a ruler (Keji Stainless Steel Ruler). The time after disconnecting the power supply until the muscle reached its initial length (70 mm) is the recovery time.

Power Consumption: The power consumption of the PTM to activate was an important feature that was measured based on the applied voltage and the characteristic of the carbon fiber provided by The Hefei Minco Heating Cable Co. the amount of consumed energy was calculated based on the formula $\frac{V^2}{R}t$ where V is the constant voltage applied on both ends of the muscle and R is the electrical resistance of the muscle, and t represents the time period from turning on the power source until the muscle reaches its highest contraction. This experiment was repeated in various condition including applying different voltage to discuss the energy and activating time required for activating the muscle.

Thermal Insulation of the Muscle: Another key aspect of the muscle features was its external temperature, which was relevant in wearable devices. During contraction on recovery of the muscle the temperature of the muscle's exterior was recorded. For this purpose, the contact thermometer integrated in HOTPLATE & MAGNETIC STIRRER PRO—ISG was used. The thermometer was attached to the PTM and the temperature was recorded

by changes in the length of the muscle to evaluate the thermal insulation of the muscle versus the contraction percentage during its activating phase.

Controllability of the Soft Joint Equipped with the PTM and Low Frequency Vibration Suspension: This characteristic was measured using a setup where the main component was the Quanser flexible joint that included a free rigid arm connected to two identical springs to provide flexibility. To measure the controllability of PTM the springs were replaced with the soft muscle and to assess low frequency vibration attenuation the PTM was added to the spring in parallel mode. The module can be derived from Matlab Simulink, but the signal must be amplified where the Quanser VoltPAQ-X1 Amplifier was exploited to amplify the driving signal. Also, for data acquisition from the flexible joint module the Quanser Q8-USB Data Acquisition device was utilized. An RL-based controller was developed (in MATLAB/SIMULINK on a common computer with the Intel Core i5-10310U Processor and 16GB RAM) in this research to control the flexible joint and while the muscle stiffness was changed, the controller was trained online to adopt to new condition. In the vibration mitigation test, while the vibration occurred the stiffness of the muscle was increased to suppress the vibration.

Supporting Information

Supporting Information is available from the Wiley Online Library or from the author.

Acknowledgements

The authors would like to thank the School of Engineering, the Faculty of Science, Engineering and Built Environment, and Deakin University for financial support.

Open access publishing facilitated by Deakin University, as part of the Wiley - Deakin University agreement via the Council of Australian University Librarians.

Conflict of Interest

The authors declare no conflict of interest.

Data Availability Statement

The data that support the findings of this study are available from the corresponding author upon reasonable request.

Keywords

4D printing, actuators, autonomy, controls, phase changes, silicone

Received: February 10, 2023

Revised: April 12, 2023

Published online:

- [1] S. K. Sood, K. S. Rawat, G. Sharma, *IEEE Trans. Eng. Manag* **2022**, <https://doi.org/10.1109/TEM.2021.3134128>.
- [2] A. Zolfagharian, A. Kaynak, M. Bodaghi, A. Z. Kouzani, S. Gharai, S. Nahavandi, *Appl. Sci.* **2020**, *10*, 3020.
- [3] J. Choi, O.-C. Kwon, W. Jo, H. J. Lee, M.-W. Moon, *3D Print. Addit. Manuf.* **2015**, *2*, 159.
- [4] X. Huang, M. Panahi-Sarmad, K. Dong, R. Li, T. Chen, X. Xiao, *Composites, Part A* **2021**, *147*, 106444.

- [5] A. Sharma, A. Rai, *Mater. Today Proc.* **2022**, <https://doi.org/10.1016/j.matpr.2022.03.679>.
- [6] S. Mallakpour, F. Tabesh, C. M. Hussain, *Adv. Colloid Interface Sci.* **2021**, *294*, 102482.
- [7] F. Momeni, X. Liu, J. Ni, *Mater. Des.* **2017**, *122*, 42.
- [8] S. Y. Hann, H. Cui, M. Nowicki, L. G. Zhang, *Addit. Manuf.* **2020**, *36*, 101567.
- [9] A. Zolfagharian, A. Kaynak, A. Kouzani, *Mater. Des.* **2020**, *188*, 108411.
- [10] M. N. I. Shiblee, K. Ahmed, M. Kawakami, H. Furukawa, *Adv. Mater. Technol.* **2019**, *4*, 1900071.
- [11] S. A. Ajwad, J. Iqbal, presented at *Int. Conf. on Engineering and Emerging Technologies (ICEET)*, Lahore, March **2015**.
- [12] S. Ajwad, M. Ullah, B. Khelifa, J. Iqbal, *J. Balk. Tribol. Assoc.* **2014**, *20*, 499.
- [13] M. Runciman, J. Avery, M. Zhao, A. Darzi, G. P. Mylonas, *Front. Rob. AI* **2020**, *6*, 141.
- [14] M. Brancadoro, M. Manti, F. Grani, S. Tognarelli, A. Menciasci, M. Cianchetti, *Front. Rob. AI* **2019**, *6*, 12.
- [15] J. Zhou, Y. Chen, Y. Hu, Z. Wang, Y. Li, G. Gu, Y. Liu, *Soft Rob.* **2020**, *7*, 743.
- [16] A. Deaconescu, T. Deaconescu, *Appl. Sci.* **2022**, *12*, 6459.
- [17] A. Zolfagharian, M. P. Mahmud, S. Gharai, M. Bodaghi, A. Z. Kouzani, A. Kaynak, *Virtual Phys. Prototyping* **2020**, *15*, 373.
- [18] W. Liao, Z. Yang, *Mater. Horiz.* **2023**, *10*, 576.
- [19] C.-H. Li, H.-Q. Wang, Z.-Y. Huang, D.-W. Yue, F.-Z. Wang, *Mater. Horiz.* **2023**.
- [20] M.-j. Kim, B.-g. Kim, J.-s. Koh, H. Yi, *Autom Constr* **2023**, *145*, 104660.
- [21] C. De Pascali, G. A. Naselli, S. Palagi, R. B. Scharff, B. Mazzolai, *Sci. Rob.* **2022**, *7*, eabn4155.
- [22] D. Sangian, S. Naficy, G. M. Spinks, *J. Intell. Mater. Syst. Struct.* **2016**, *27*, 2508.
- [23] E. Sun, T. Wang, *Smart Mater. Struct.* **2019**, *28*, 127001.
- [24] S. M. Mirvakili, D. Sim, I. W. Hunter, R. Langer, *Sci. Rob.* **2020**, *5*, eaaz4239.
- [25] C. Tawk, G. Alici, in *Smart Materials in Additive Manufacturing, Volume 2: 4D Printing Mechanics, Modeling, and Advanced Engineering Applications*, Elsevier, New York **2022**, pp. 103–140.
- [26] I. H. Akyuz, E. Yolacan, H. M. Ertunc, Z. Bingul, in *2011 IEEE Int. Conf. on Mechatronics*, IEEE, Piscataway, NJ, **2011** pp. 409–414.
- [27] M. Ahmad, M. Suid, M. Ramli, M. Zawawi, R. R. Ismail, in *2010 6th Int. Colloquium on Signal Processing & its Applications*, IEEE, Piscataway, NJ **2010**, pp. 1–5.
- [28] M. A. Ahmad, in *2008 Second UKSIM European Symp. on Computer Modeling and Simulation*, IEEE, Piscataway, NJ, **2008**, pp. 40–45.
- [29] C. Chitu, J. Lackner, M. Horn, H. Waser, M. Kohlböck, in *Proc. of the Joint INDS'11 & ISTET'11*, IEEE, Austria **2011**, pp. 1–5.
- [30] J. Ju, Y. Zhao, C. Zhang, Y. Liu, *Algorithms* **2018**, *11*, 189.
- [31] S. M. Ahmadi, M. M. Fateh, *Trans. Inst. Meas. Control* **2019**, *41*, 4023.
- [32] H. Ahmadian, H. A. Talebi, I. Sharifi, in *2020 28th Iranian Conference on Electrical Engineering (ICEE)*, IEEE, Piscataway, NJ **2020**, pp. 1–6.
- [33] P. Sarkhel, N. Banerjee, N. B. Hui, *SN Appl. Sci.* **2020**, *2*, 1124.
- [34] W. He, Z. Yan, Y. Sun, Y. Ou, C. Sun, *IEEE Trans. Neural Networks Learn. Syst.* **2018**, *29*, 5993.
- [35] B. Subudhi, A. S. Morris, *Appl. Soft Comput.* **2009**, *9*, 149.
- [36] S. K. Pradhan, B. Subudhi, *IEEE Trans. Autom. Sci. Eng.* **2012**, *9*, 237.
- [37] T. Long, E. Li, Y. Hu, L. Yang, J. Fan, Z. Liang, R. Guo, *IEEE Trans. Neural Networks Learn. Syst.* **2020**, *32*, 841.
- [38] D. Sendrescu, G. Bujgoi, D. Chintescu, in *2020 21th Int. Carpathian Control Conf. (ICCC)*, IEEE, Piscataway, NJ **2020**, pp. 1–5.
- [39] D. Pavlichenko, S. Behnke, *arXiv:2203.07051* **2022**.
- [40] M. Mohammadi, A. Zolfagharian, M. Bodaghi, Y. Xiang, A. Z. Kouzani, *Bio-Des. Manuf.* **2022**, *5*, 786.
- [41] Y. S. Narang, B. Aktaş, S. Ornellas, J. J. Vlassak, R. D. Howe, *Soft Rob.* **2020**, *7*, 724.